# Modeling the Propeller Slipstream Effect on Lift and Pitching Moment

Bouquet, Thijs; Vos, Roelof

**DOI**
10.2514/6.2017-0236

**Publication date**
2017

**Document Version**
Accepted author manuscript

**Published in**
55th AIAA Aerospace Sciences Meeting

This is an Accepted Manuscript of an article published in: 55th AIAA Aerospace Sciences Meeting, 9/01/17 - 13/01/17 Grapevine, USA ISBN: 978-1-62410-447-3
Available online: https://arc.aiaa.org/doi/10.2514/6.2017-0236

# Modeling the Propeller Slipstream Effect on Lift and Pitching Moment

Thijs Bouquet* and Roelof Vos†
*Delft University of Technology, Delft, 2600AA, the Netherlands*

**A semi-analytical prediction method is presented to predict the effect of the propeller slipstream on the lift and pitching moment of a propeller-powered aircraft. The method assesses three effects caused by the propeller slipstream: an increase in lift over the wing due to the slipstream, a change in the tail-off pitching moment, and a change in the horizontal tail contribution to the pitching moment due to increased downwash and (possibly) dynamic pressure. This prediction method is validated using wind tunnel data for the Fokker 50 and a special version of the Saab 340 with T-tail. The prediction method shows good correlation with the experimental results for various combinations of flap deflection, angle-of-attack, and thrust coefficient. Further analysis of the results demonstrates that the propeller slipstream effect reduces the tail effectiveness due to an increase in downwash gradient at the horizontal tail. Furthermore, it is shown that the effectiveness of the tail is influenced by the vertical position of the tail with respect to the slipstream due to slipstream inflow and a (possible) change dynamic pressure ratio.**

## I. Introduction

The implementation of propeller engines has significant implications with respect to the stability and control of an aircraft. Due to the increased flow velocity over the wing and a propeller normal force, the pitching moments change due to the presence of a propeller slipstream. Furthermore, the increasing downwash and potential increase in dynamic pressure over the tail also changes the effectiveness of the horizontal tail. These changes must be taken into account to accurately determine the minimal horizontal tail surface area. The complex nature of the propeller slipstream effect means that these implications are normally not incorporated in the conceptual design phase. As Phillips[1] says, "The effects of the propeller slipstream on other airplane surfaces such as the wing, tail and fuselage are very complex and do not lend themselves to accurate analytical treatment. These effects can be accurately evaluated only from powered wind tunnel tests. Such tests are commonly performed in the final phase of the airplane design process. Simply because of complexity, the slipstream effects are usually neglected in the preliminary design phase. It should be remembered, however, that the slipstream effects can be significant." Therefore, the question that this paper is trying to answer is, "How can the propeller slipstream effect on the longitudinal stability and control of a conventional aircraft be predicted quickly during the preliminary design phase?"

Figure 1 illustrates the helical vortex system resulting from a propeller blade advancing through the flow. The helical vortex system tends to deform and roll-up, producing a slipstream tube with strong variations in flow quantities. Although the slipstream can be described using many variables, only the following variables are discussed in further detail as these are relevant for the modeling of the slipstream in relation to the topic of this paper: (1) Axial and swirl velocity profiles, (2) Contraction, and (3) installed propeller effects on the wing.

When examining velocity profiles of an uninstalled propeller, the axial velocity ($v_a$) is determined as the velocity along the propeller thrust axis. The axial velocity varies along the propeller blade, with a maximum at roughly 3/4 of the radius. The maximum occurs at this position as the blade loading is also maximum

*MSc Student, Faculty of Aerospace Engineering, Delft University of Technology, P.O. Box 5058, 2600 GB Delft, The Netherlands
†Assistant Professor, Faculty of Aerospace Engineering, Delft University of Technology, P.O. Box 5058, 2600 GB Delft, The Netherlands, Senior Member AIAA

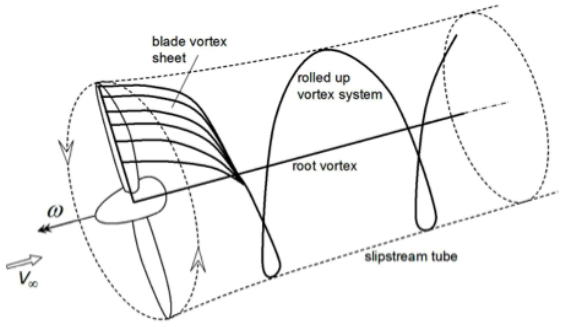


**Figure 1. Helical vortex system and slipstream tube generated by propeller[2]**

at this location. The axial velocity in the propeller slipstream increases downstream of the propeller. This means that the longitudinal distance between the propeller and a downstream location in the streamtube has an important effect on the local axial velocity magnitude.The swirl velocity ($v_t$) is the propeller induced tangential velocity. The swirl velocity profile in the longitudinal direction is shown in Figure 2(b). It is assumed that the swirl velocity remains unchanged with longitudinal position.

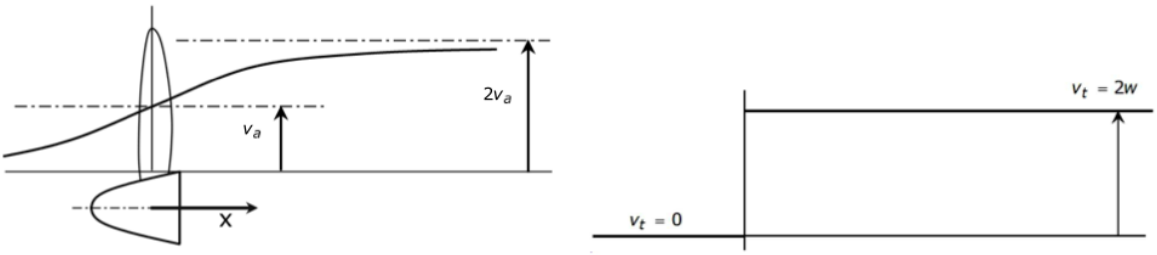


(a) Axial velocity

(b) Swirl velocity

**Figure 2. Velocity variations induced by the propeller.[2]**

For the uninstalled propeller, the streamtube is assumed to be circular with the same radius as the propeller at the propeller location. Further downstream the streamtube contracts to maintain constant mass flow as the axial velocity increases. For the uninstalled propeller, the contraction ratio $R_S/R$ can be approximated using the following equation as determined by Theodorsen:[3]

$$\frac{R_S(x)}{R} = \sqrt{\frac{1+a}{1+a\left(1+\frac{x}{\sqrt{R^2+x^2}}\right)}} \tag{1}$$

Where $a$ is defined as the dimensionless axial velocity factor $\left(\frac{v_a}{V_0}\right)$.

The installed propeller effects on the wing schematically shown in Figure 3. As the flow is accelerated in axial direction by the propeller, the dynamic pressure over the wing is increased, resulting in an increase in local lift. Due to the rotation of the propeller the upward rotating blade causes an increase in local angle-of-attack on the wing resulting from the swirl velocity. In the same manner, the downward rotating blade position produces a lower local angle-of-attack on the wing. This change in local angle-of-attack causes a respective increase or decrease in local lift coefficient as shown in the figure. The importance of rotation direction is also shown by illustrating the placement of the local lift coefficient peak at the upward rotating side in the inboard or outboard rotating case. Figure 3 shows the combination of these effects on the lift distribution over the wing and demonstrate the effect of rotational direction.

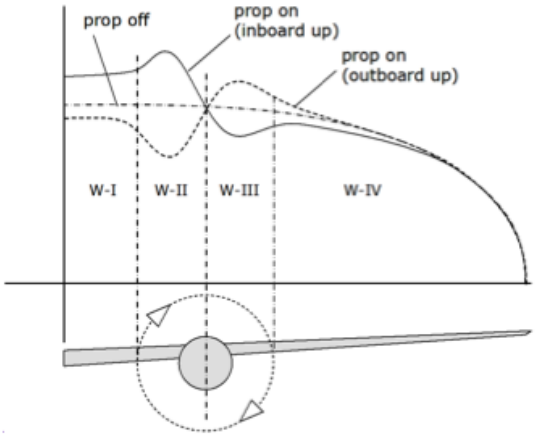


**Figure 3. Lift distribution over the wing as affected by the slipstream[2]**

The remaining part of this paper is structured as follows. The relevant theory regarding propeller engines, the theory of slipstream effect on lift and pitching moment in Section II. The the prediction method is compared to experimental results in Section III. The results of the prediction method are further interpreted in Section IV Finally, conclusions and recommendations following from this investigation are given in Section V.

## II. Analysis Methodology

The method to predict the effect of the propeller slipstream on the longitudinal stability and control is based the method of Obert.[4] This method has been expanded to determine required variables which are not available from windtunnel data. The additions to the method will be detailed in their corresponding subsections. The following assumptions are made:

- The slipstream rotation (swirl) and directional translation can be neglected
- The slipstream cross-section remains circular with the contracted slipstream diameter at the horizontal tail
- For the determination of the tail-off lift coefficient, the axial velocity is considered to be uniform across the slipstream section

### A. Tail-off lift coefficient

The total tail-off lift coefficient ($C_{L_{\text{T-O}}}$) is the sum of the lift coefficient due to the wing plus slipstream ($C_{L_{\text{W+S}}}$), the lift due to the propeller normal force ($C_{L_{\text{P}}}$), and a thrust component perpendicular to the free stream direction ($C_{L_{\text{T}}}$):

$$C_{L_{\text{T-O}}} = C_{L_{\text{W+S}}} + C_{L_{\text{P}}} + C_{L_{\text{T}}} \tag{2}$$

The lift due to thrust is computed as follows:

$$C_{L_T} = C_T \sin\alpha \quad \text{with} \quad C_T = \frac{T}{\frac{1}{2}\rho V^2 S} \tag{3}$$

The lift due to the propeller normal force is computed by following the method of de Young,[5] which is documented in ESDU data sheet 89047[6] with reference to ESDU data sheet 85015[7] for the computation of propeller installation parameters.

To determine the change in lift over the wing due to the propeller slipstream, a method developed by Stepniewsky[8] which incorporates lifting line theory, was used. According to lifting line theory, the lift on a wing can be determined using:[4]

$$L_{\text{W}} = \dot{m}_0 V_0 \sin\varepsilon = \rho\frac{\pi}{4} b_{\text{W}}^2 V_0^2 \sin\varepsilon \tag{4}$$

This equation states that the flow can be considered as a stream tube with circular cross section and diameter equal to the span of the wing which is deflected over the downwash angle ($\varepsilon$). Stepniewsky expanded on this by stating that the lift due to propeller slipstream is equal to the momentum resulting from the downward deflection of each streamtube of the propeller slipstream deflected over the slipstream downwash angle ($\varepsilon_S$):[8]

$$L_S = n_e \dot{m}_S (V_0 + \Delta V) \sin \varepsilon_S = n_e \rho \frac{\pi}{4} D^{*2} (V_0 + \Delta V)^2 \sin \varepsilon_S \tag{5}$$

In this equation, $D^*$ is the contracted slipstream diameter. The contracted slipstream diameter is dependent on the propeller diameter, freestream flow velocity and velocity increase over the propeller blade as given by Roskam:[9]

$$D^* = D \sqrt{\frac{V_0 + \Delta V/2}{V_0 + \Delta V}} \tag{6}$$

Furthermore, the velocity increase in the fully contracted slipstream ($\Delta V$) can be calculated using:

$$\frac{\Delta V}{V_0} = \frac{V_e - V_0}{V_0} = \sqrt{1 + C_T \frac{S_W}{n_e \frac{\pi}{4} D^2}} - 1 \tag{7}$$

To calculate the lift over a wing with slipstream present, the total cross-sectional area of the contracted slipstream tubes needs to be subtracted from the cross-sectional area describing the outer flow. Doing so gives the lift over a wing (W) with a propeller slipstream (S) present:

$$L_{W+S} = \rho V_0^2 \left[ \frac{\pi}{4} b_W^2 - n_e \frac{\pi}{4} D^{*2} \right] \sin \varepsilon + \rho [V_0 + \Delta V]^2 n_e \frac{\pi}{4} D^{*2} \sin \varepsilon_S \tag{8}$$

The corresponding lift coefficient is:

$$C_{L_{W+S}} = \frac{L_{W+S}}{\frac{1}{2} \rho V_0^2 S_W} = \frac{2}{S_W} \left( \frac{\pi}{4} b_W^2 - n_e \frac{\pi}{4} D^{*2} \right) \sin \varepsilon + n_e \frac{\pi D^{*2}}{2 S_W} \frac{(V_0 + \Delta V)^2}{V_0^2} \sin \varepsilon_S \tag{9}$$

The downwash due to slipstream ($\varepsilon_s$) is estimated by using the assumption that the lift due to slipstream is equal to the lift on a wing in free flow with a span equal to the diameter of the fully contracted slipstream and an airfoil section equal to the wing section at the propeller axes with flaps deflected.[4] Combining this assumption with lifting line theory gives:

$$\sin \varepsilon_S = \frac{2 C_{L_{\alpha_{s,\text{eff}}}}}{\pi A_{s,\text{eff}}} \sin \alpha_S \tag{10}$$

The effective aspect ratio of the wing part immersed in the slipstream ($A_{S_{\text{eff}}}$) is dependent on the thrust coefficient. It is computed using:

$$A_{S_{\text{eff}}} = A_S + (A_W - A_S) \left( \frac{V_0}{V_0 + \Delta V} \right)^{(A_W - A_S)} \tag{11}$$

The effective lift-curve slope of the slipstream section of the wing $\left( C_{L_{\alpha_{s,\text{eff}}}} \right)$ is found using Figure 4 from NACA report 1098.[10] The angle-of-attack of this section ($\alpha_s$) is the angle between the effective propeller slipstream center line and the zero-lift angle-of-attack with flaps deflected:

$$\alpha_S = \alpha^* + i_{c_S} - \alpha_0 - \Delta \alpha_{0,f} \tag{12}$$

where $i_{c_S}$ is the angle of incidence of the local wing chord with respect to the fuselage reference line, $\alpha_0$ is the zero-lift angle-of-attack of the relevant airfoil section, and $\Delta \alpha_{0,f}$ is the change in zero-lift angle-of-attack due to flap deflection. Finally, the change in flow direction due to the acceleration of the flow at the propeller disk, $\alpha^*$, is calculated using:

$$\alpha^* = \arctan \frac{V_0 \sin \alpha_R}{V_0 \cos \alpha_R + \Delta V/2} \tag{13}$$

where $\alpha_R$ is the aircraft angle-of-attack.

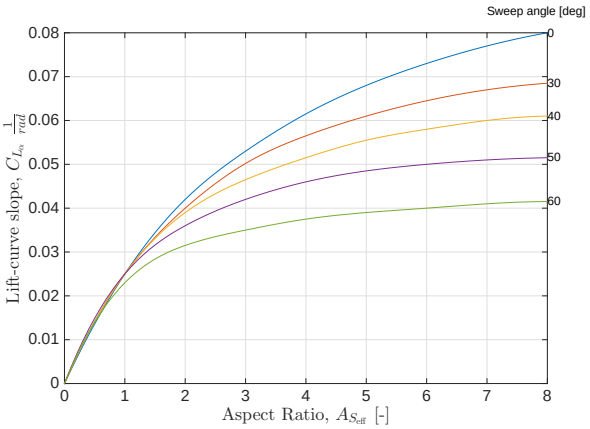


**Figure 4. Variation of lift-curve slope with aspect ratio, and sweepback for subsonic incompressible flow[10]**

The downwash directly behind the wing without propeller slipstream, $\varepsilon$, is found from lifting line theory:

$$\sin\varepsilon = \frac{2C_{L_\mathrm{W}}}{\pi A_\mathrm{W}} \tag{14}$$

In this equation, the power-off lift coefficient of the wing, $C_{L_\mathrm{W}}$ is found by modeling the wing with the vortex-lattice method AVL.[11] The lift coefficient due to propeller slipstream can be calculated using:

$$C_{L_\mathrm{S}} = C_{L_{\mathrm{W+S}}} - C_{L_\mathrm{W}} \tag{15}$$

## B. Tail-Off Pitching Moment

The pitching moment of aircraft-less-tail with thrust-producing propellers is a summation of the pitching moment at zero thrust ($C_{m_{C_T=0}}$), the pitching moment due to the propeller normal force ($C_{m_\mathrm{P}}$), the pitching moment due to the change in thrust vector ($C_{m_\mathrm{T}}$), and the pitching moment due to the slipstream effect ($C_{m_\mathrm{S}}$). In the subsequent paragraphs, all pitching moments are taken about the reference point of the aircraft, which is the quarter-chord of the mean aerodynamic chord, i.e. $\bar{c}/4$. The pitching moment coefficient of the aircraft-less-tail is:

$$C_{m_{\text{T-O}}} = C_{m_{C_T=0}} + C_{m_\mathrm{P}} + C_{m_\mathrm{T}} + C_{m_\mathrm{S}} \tag{16}$$

The slipstream effect on pitching moment is caused by the change in flow velocity over the wing in the propeller slipstream ($C_{m_\mathrm{S}}$). The following contributions are distinguished: a contribution due to the slipstream effect on the clean wing ($C_{m_{\mathrm{S},0}}$), a contribution due to the slipstream and flap deflection at constant angle-of-attack ($C_{m_{\mathrm{S},\delta_f}}$), and a contribution due to angle-of-attack at constant flap deflection, $C_{m_{\mathrm{S},\alpha}}$.

$$C_{m_\mathrm{S}} = C_{m_{\mathrm{S},0}} + \Delta C_{m_{\mathrm{S},\delta_f}} + \Delta C_{m_{\mathrm{S},\alpha}} \tag{17}$$

Starting with the clean wing, the contribution to the pitching moment of the propeller slipstream can be computed as:

$$C_{m_{\mathrm{S},0}} = n_e \frac{D^* c_\mathrm{s}}{S_\mathrm{W}} c_{m_{0,\mathrm{s}}} \left[ \left( \frac{V_0 + \Delta V}{V_0} \right)^2 - 1 \right] \tag{18}$$

where $c_{m_{0,\mathrm{s}}}$ is the local pitching moment coefficient of the airfoil located on the propeller axis. For clean wings, the increase in lift due to propeller slipstream is assumed to apply at the quarter-chord point of the local chord in line with the propeller axis ($c_s$). When flaps are deflected, the change in lift coefficient is applied to the extended chord ($c'_s$). Based on numerous windtunnel test results, Obert expanded Glauert's theoretical relation for hinged flaps to the following equation:[4]

$$\Delta C_{m_{\mathrm{S},\,\delta_f}} = \frac{c'_s}{c_s} \left[ -0.25 + 0.32 \frac{c_\mathrm{f}}{c'_s} \right] \left[ 1 + 0.2 \left( 1 - \sqrt{2} \sin\delta_\mathrm{f} \right) \right] \Delta C_{L_{\mathrm{S},\delta_f}} \tag{19}$$

where

$$\Delta C_{L_{\mathrm{S},\delta_f}} = C_{L_\mathrm{S}} - C_{L_\mathrm{S}}|_{\delta_f=0} \tag{20}$$

The change in pitching moment about the quarter-chord point of the extended chord due to lift caused by the propeller slipstream at angle-of-attack ($\Delta C_{m_{\mathrm{S},\alpha}}$) is determined using:

$$\Delta C_{m_{\mathrm{S},\alpha}} = F \times \Delta C_{L_{\mathrm{S},\alpha}} \tag{21}$$

with

$$F = \begin{cases} \left\{ \left[ \frac{0.5\delta_f}{30} + 0.25 \right] \left( \frac{c'_s}{c_s} - 1 \right) + 0.05 \frac{\delta_f}{30} + \frac{\Delta X_{\mathrm{fus}}}{\bar{c}} \left( 1 - \frac{\delta_f}{30} \right) \right\} & \text{for } 0 \leq \delta_f \leq 30 \\ -0.75 \left( \frac{c'_s}{c_s} - 1 \right) - 0.05 \quad \text{for } \delta_f > 30 \end{cases} \tag{22}$$

and

$$\Delta C_{L_{\mathrm{S},\alpha}} = C_{L_\mathrm{S}} - C_{L_\mathrm{S}}|_{\alpha=0} \tag{23}$$

where $\Delta X_{\mathrm{fus}}$ is representing a contribution of the fuselage to the shift in lift-force application point.[12]

## C. Tail-On Pitching Moment

The tail-on pitching moment ($C_m$) is calculated by adding the horizontal tail pitching moment ($\Delta C_{m_\mathrm{h}}$) to the previously calculated tail-off pitching moment, or simply:

$$C_m = C_{m_{\mathrm{T\text{-}O}}} + C_{m_\mathrm{h}} \tag{24}$$

where the horizontal tail pitching moment is computed as follows using:

$$C_{m_\mathrm{h}} = -\left(\alpha_R - \varepsilon + i_\mathrm{h}\right) C_{L_{\alpha,\mathrm{h}}} \frac{q_\mathrm{h}}{q} \frac{S_\mathrm{h} l_\mathrm{h}}{S_\mathrm{W} \bar{c}} \tag{25}$$

where $i_\mathrm{h}$ is the incidence angle of the horizontal tail, $C_{L_{\alpha,\mathrm{h}}}$ its lift curve slope, $\frac{q_\mathrm{h}}{q}$ the ratio of dynamic pressure at the horizontal tail, and $\frac{S_\mathrm{h} l_\mathrm{h}}{S_\mathrm{W} \bar{c}}$ the tail volume coefficient (with $l_\mathrm{h}$ being the horizontal distance between the quarter chord points of the wing's and horizontal tail plane's mean aerodynamic chords). While the lift-curve slope is found using a vortex-lattice method (AVL), the local downwash angle ($\varepsilon$) and local dynamic pressure ($q_\mathrm{h}$) need further elaboration. For both computations, the location of the slipstream center line with respect to the horizontal tail plane needs to be determined.

### *1. Vertical Distance of Slipstream Center Line to Horizontal Tail*

The distance $h$ between the slipstream center line and the horizontal tail consists of four contributions: the geometrical distance between the tail surface and the propeller axis at zero angle-of-attack, the vertical displacement of the horizontal tail due to angle-of-attack, the vertical displacement of the slipstream center line passing through the clean wing's trailing edge, and the vertical displacement of the slipstream center line due to the propeller axis not coinciding with the streamline leading to the forward stagnation point. This final contribution itself comprises of three components: the displacement of the propeller disk due to angle-of-attack with respect to the quarter chord reference point, the displacement of the center line due to the downward displacement of the trailing edge when flaps are deflected, and the displacement of the centerline caused by upwash in front of the wing due to flap deflection. The following equation is sums all these distances to find the slipstream center line and the horizontal tail:[4]

$$h = z_\mathrm{h} - z_{\mathrm{prop}} - l_\mathrm{h} \sin\alpha + l^*_\mathrm{h} \sin\left(K_\varepsilon \varepsilon\right) - \left(x_{\bar{c}/4} - x_{\mathrm{prop}}\right) \sin\alpha + c_f \sin\delta_f + 0.25 \left[x_{\bar{c}/4} - x_{\mathrm{prop}}\right] \sin\Delta\alpha_{0,f} \tag{26}$$

where $z$ indicates vertical position of a component in the aircraft reference frame, $\Delta\alpha_{0,f}$ is the change in airfoil section zero-lift angle-of-attack due to flap deflection (obtained using AVL), and $K\varepsilon$ is an empirical downwash factor ($K_\varepsilon = z_\mathrm{W}/z_\varepsilon$). The latter is related to the horizontal distance between the wing trailing edge and horizontal-tail leading edge ($l^*_\mathrm{h}$) according to the curve shown in Figure 5. This factor accounts for the fact that the slipstream center line continues to curve downwards downstream of the wing. In this equation, the downwash ($\varepsilon$) is calculated assuming no inflow effects, which will be described in the following subsection.

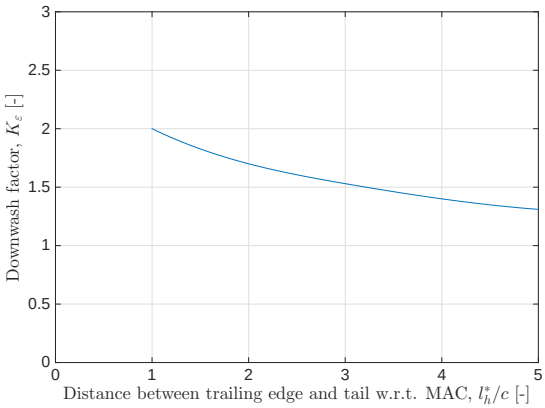


**Figure 5. Downwash factor $K_\varepsilon$ versus distance behind the wing trailing edge.[4]**

*2. Downwash*

The downwash behind a wing with rotating propellers is assumed to consist of three major components: the power-off downwash resulting primarily from lift over the wing (computed with AVL), the change in downwash due to the increase in lift over the wing by propeller slipstream, and an inflow from the external flow into the slipstream. The last component only occurs when the distance between the horizontal tail and the slipstream center line is less that 1.25 times the contracted slipstream diameter ($D^*$). The downwash increases or decreases depending on whether the tail is above or below the slipstream center line, respectively. The downwash due to inflow is dependent on the increase in flow velocity in the contracted slipstream with respect to the freestream velocity $\left(\frac{\Delta V}{V_0}\right)$. The downwash at the horizontal tail is computed as follows:[4]

$$\varepsilon = (\varepsilon_0)_{\text{P-O}} + \left(\frac{\mathrm{d}\varepsilon}{\mathrm{d}C_L}\right)_{\text{P-O}} (C_{L_{\text{P-O}}} + C_{L_{\text{S}}}) + (\Delta\varepsilon)_{\frac{\Delta V}{V_0}=1} \left(\frac{\Delta V}{V_0}\right) \tag{27}$$

Here, the downwash at the zero-lift angle-of-attack $[(\varepsilon_0)_{\text{P-O}}]$ is a result of the fact that although the total lift is zero, the flow behind the wing is not necessarily the same as the undisturbed flow (i.e. due to a non-elliptical lift distribution or upwash from the fuselage or nacelles). In the current implementation, these effects are ignored, i.e. the subscripts "P-O" can be replaced with "W". The curve for $(\Delta\varepsilon)_{\frac{\Delta V}{V_0}=1}$ was determined empirically as a function of the previously mentioned distance between slipstream center line and horizontal tail ($h$). This curve is shown in Figure 6.

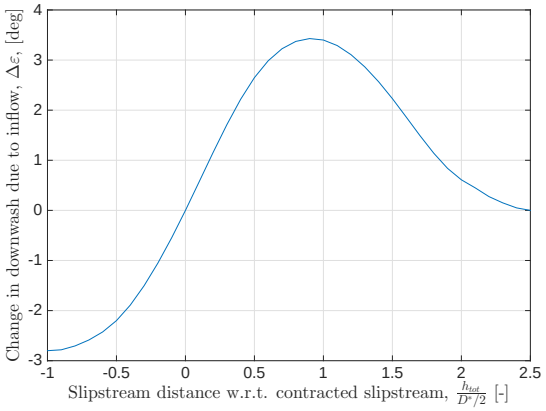


**Figure 6. Change in downwash at the tailplane due to inflow into the slipstream - generalized curve[4]**

*3. Average Dynamic Pressure*

The average dynamic pressure at the horizontal tail ($q_h$) is determined by calculating the tail area covered by the propeller streamtubes. This area can be determined using the situation sketched in Figure 7. The tail area can be determined as:

$$S_{\mathrm{S}} = 2 b_{\mathrm{S}} c_{h_{\mathrm{s}}} \tag{28}$$

where the span of the tail covered by the slipstream is found using:

$$b_{\mathrm{S}} = D^* \sqrt{1 - \left(\frac{2h}{D^*}\right)^2} \tag{29}$$

The average dynamic pressure at the tail can then be found using the assumption that no mixing occurs between the slipstream and outer flow. Under this assumption, the dynamic pressure ratio is:[4]

$$\frac{q_h}{q} = \left[\left(1 + \frac{\Delta V}{V_0}\right)^2 \frac{S_{\mathrm{h,S}}}{S_{\mathrm{h}}} + \left(1 - \frac{S_{\mathrm{h,S}}}{S_{\mathrm{h}}}\right)\right] \tag{30}$$

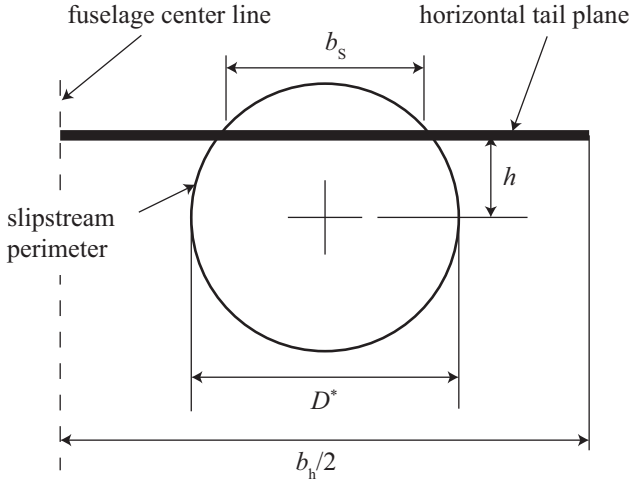


**Figure 7. Tail span covered by the propeller slipstream**

## III. Method Verification

Little validation data exists in the open literature to validate the presented method. The only useable data sets that could be found are for the Fokker 50[4] and Saab 340 with a T-tail configuration[13] (referred to as Saab 340T) . The dimensions for the Saab 340T were used as direct inputs for the method. The Fokker 50I design was synthesized using the Initiator and therefore demonstrates the applicability of the method as part of an aircraft synthesis program. Table 1 shows the difference in aircraft dimensions of the synthesized aircraft versus the actual dimensions of the Fokker 50.

**Table 1. Dimensions of synthesized propeller aircraft compared to actual Fokker 50 dimensions**

| Dimension | Actual Fokker 50 | Initiator Fokker 50I | Difference |
|---|---|---|---|
| Fuselage Length [m] | 25.25 | 24.1 | -4.5% |
| Wing Area [$m^2$] | 70 | 68.3 | -2.4% |
| Wing Span [m] | 29 | 28.6 | -1.3% |
| Propeller Diameter [m] | 3.66 | 3.64 | -0.4% |

## A. Tail-off Lift Coefficient

The tail-off lift curves show the tail-off lift coefficient ($C_{L_{\text{T-O}}}$) versus angle-of-attack at various propeller thrust coefficients and flap deflections. The tail-off lift curves for the Saab 340T at various flap deflections and propeller thrust coefficients are shown in Figure 8(a). This figure shows a good correlation between the calculated values and the windtunnel test results although the individual contributions of flap deflection and thrust cannot be discerned. Instead, Figure 8(b) gives a clearer indication of the propeller slipstream effect on the lift curves. This figure shows the difference between the tail-off lift-curve slopes in the power-off and power-on ($C_T = 0.6$) condition at a constant flap deflection of 20 degrees. For example, at $\alpha = 0$ the lift coefficient is increased by roughly 35%, proving the significant of the propeller slipstream. Furthermore, the figure again shows a good correlation between the measured and calculated results.

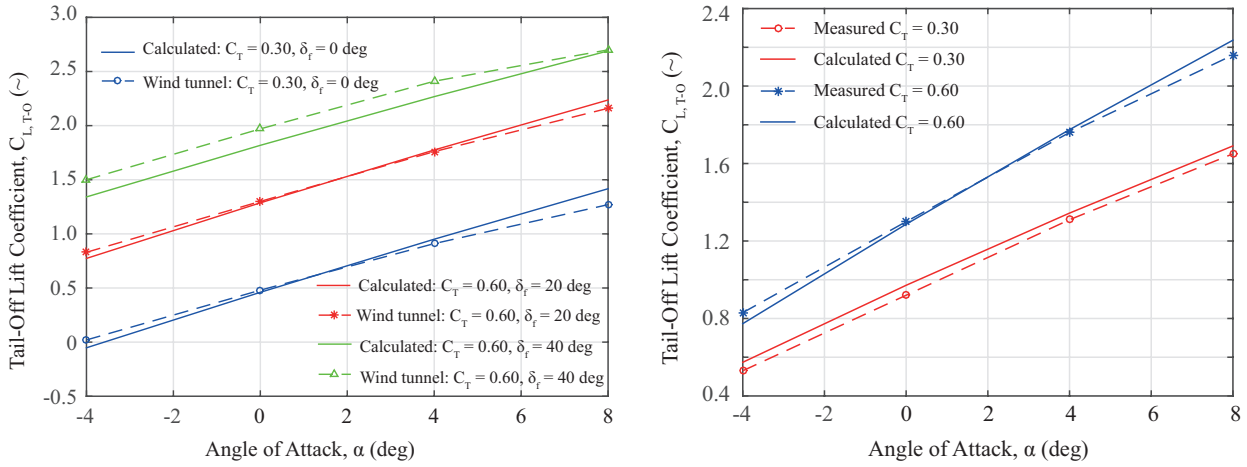


(a) Flaps 0, 20, 40 degrees

(b) Flaps 20 degrees

**Figure 8. Tail-off lift curves - Saab 340T**

Figure 8(a) shows that the lift is predicted with a maximum discrepancy of 11% in lift coefficient occurring at 40degrees flap deflection. The main error in all three flight settings is that the lift curve slope is slightly steeper compared to the test data. This error could be causes by an over prediction of the lift curve slope by AVL, the propeller normal force slope, or the slipstream effect. From Figure 8(b) the conclusion can be drawn that the lift curve slope as predicted by AVL is correct, albeit with a constant offset.

Figure 9 contains the lift curves at a constant flap deflection angle for increasing thrust coefficients of the Fokker 50I. These figures again clearly show the increase in tail-off lift, due to propeller thrust as the lift curve slopes are steeper for higher thrust coefficients. Furthermore, as expected, the tail-off lift is higher at higher flap deflections.

The curves for the Fokker 50I show similar effects as the Saab 340T. In general, the calculated values coincide reasonably well with the measured values. However, a comparatively larger error occurs with respect to the Saab 340T. A larger error is expected because the Fokker 50I calculations are based on the aircraft dimensions which follow from the Initiator design (see Table 1). The larger error can be observed when comparing the power-off lift curves in Figure 9 to the power-off lift curve of the Saab 340T. When comparing the propeller slipstream contributions, the calculations seem to slightly over predict the effect. This can be seen as the calculated curves increase relatively compared to the measured curves. Although this means that the calculated values correlate better with the measured values in some cases (Figure 9(d)), this does not mean that this is correct. The over prediction is in line with the results for the Saab 340T, and could thus be credited to a number of effects including an erroneous increase in propeller normal force or incorrect effective lift slope for the slipstream section.

## B. Pitching Moment Coefficient

The pitching moment curves, indicating the tail-off and tail-on pitching moments about a certain reference point versus the corresponding lift coefficient, are given per aircraft. Again the Saab 340T results are presented first, followed by the Fokker 50I. These figures were found by determining the lift coefficient and

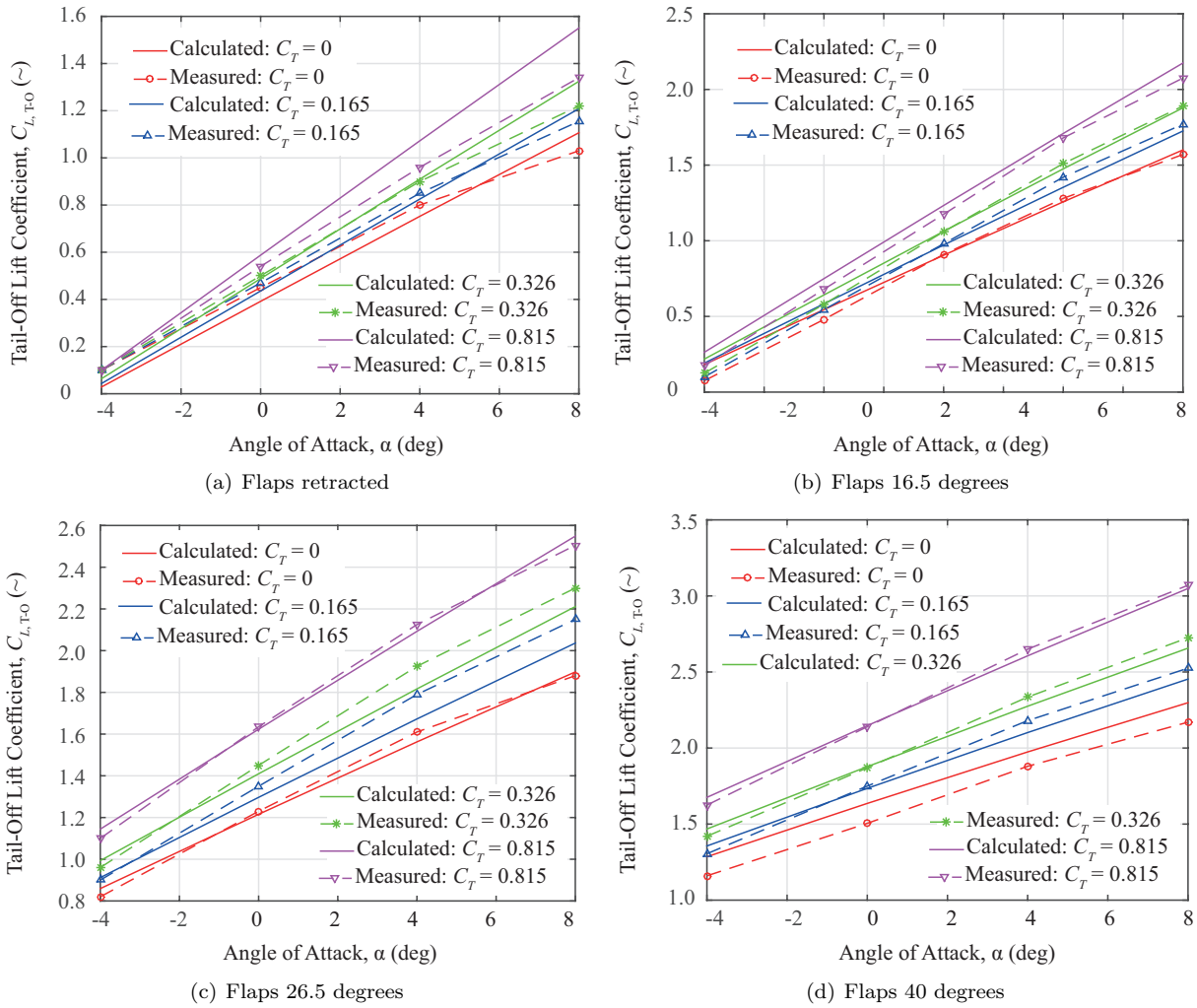


(a) Flaps retracted

(b) Flaps 16.5 degrees

(c) Flaps 26.5 degrees

(d) Flaps 40 degrees

**Figure 9. Tail-off lift curves - Fokker 50I**

pitching moments at various angles of attack. As a result, constant angles of attack lines are also shown between the power-off and power-on lines to indicate the change in lift and pitching moment due to rotating propellers. It should be noted that the power-off tail-off moments were taken from the wind tunnel data.

Three pitching moment graphs are shown for the Saab 340T in Figure 10. Both the tail-off and tail-on pitching moments are shown. The tail-off pitching moment curves show two major effects due to propeller thrust. The first is the increasing lift coefficient due to the propeller slipstream. The second is an overall decrease in pitching moment. This effect effect however reduces for higher angles of attack, and even becomes positive when flaps are retracted. The tail-on curves here are shown primarily to validate the downwash prediction method.

Starting off by examining the tail-off pitching moments, the implemented method using the AVL input seems to follow the trend of the wind tunnel results well. In fact, the over prediction of the AVL input compared to the wind tunnel data mentioned earlier in Figure 8(b), seems to increase the accuracy of the propeller slipstream prediction. This suggests that the implemented calculation is under predicting the change in pitching moment. However, this under prediction is being compensated by a slight over prediction in lift by AVL. The maximum error for the tail-off pitching moment is less than 10% and as such the implemented method still adequately predicts the pitching moment in the conceptual design phase.

The tail-on pitching moments show the largest error of the validation results thus far. A (partial) reason for this is that the tail-on pitching moment is computed using many variables calculated upstream, which implies that any foregoing errors are carried over to the results. Secondly, as mentioned in Section C, the assumption is made that the downwash due to propeller slipstream is caused only by the lift increase over

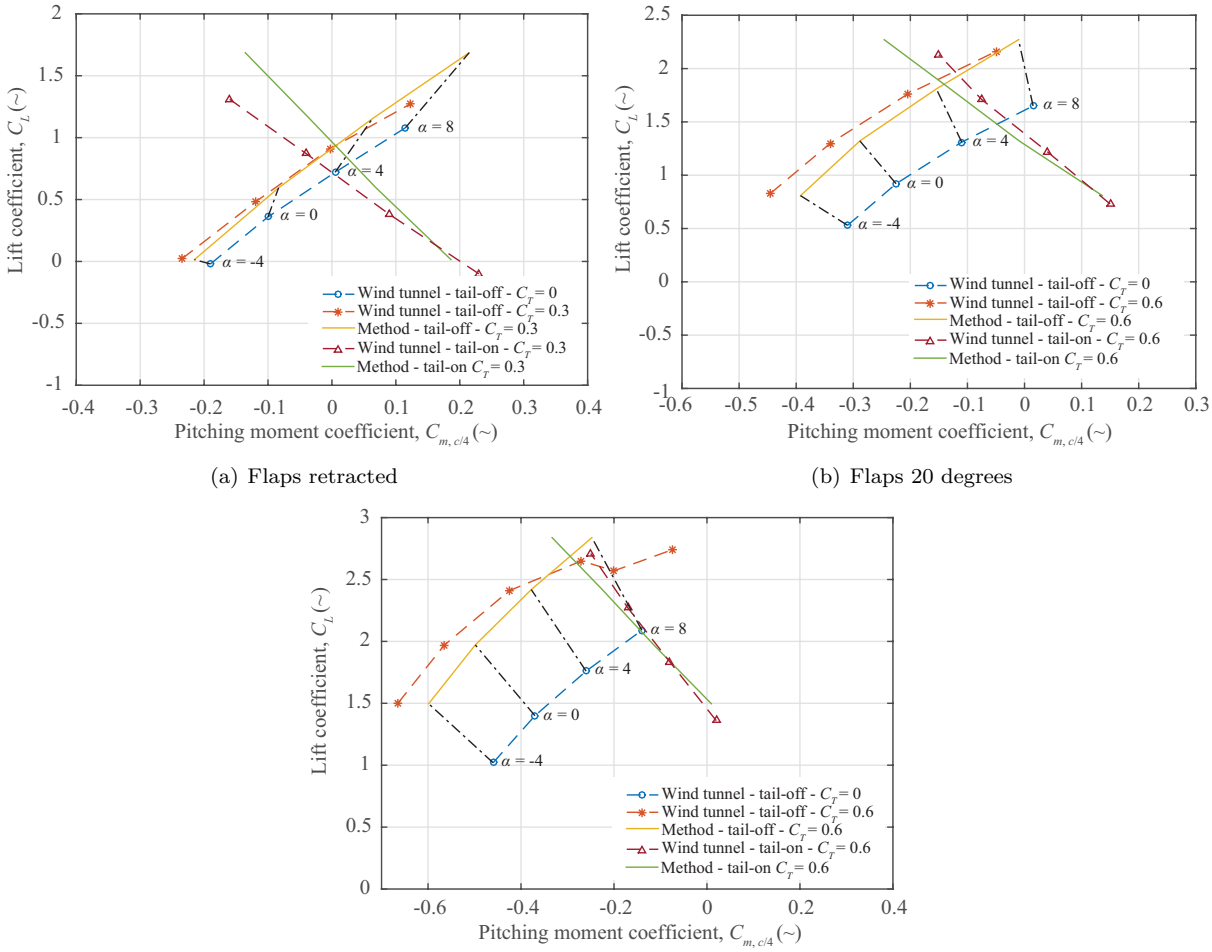


(a) Flaps retracted

(b) Flaps 20 degrees

(c) Flaps 40 degrees

**Figure 10. Pitching moment curves - Saab 340T**

the wing due to the slipstream. Although this assumption seems valid, it remains a simplification which could lead to inherent inconsistencies. Finally, the implemented downwash prediction is based on AVL computations which also contain minor errors as shown in Jansen and Vos.[14] Despite these errors, the implemented method using AVL input still predicts the tail-on pitching moment with sufficient accuracy for the conceptual design phase of a propeller aircraft.

For the Fokker 50I, the obtained results are shown in Figure 11. These graphs show the tail-off pitching moment curves at flap deflections of 16.5 degrees and 40 degrees. No validation data was found for tail-on curves. The curves were computed in the same manner as for the Saab 340T, in that the lift coefficients and pitching moment coefficients were computed at various angles of attack. Both figures show similar effects as the Saab 340T. For increasing thrust coefficient, the tail-off lift coefficient increases as expected. The tail-off pitching moment also becomes more negative at higher thrust.

The tail-off pitching moment curves for the Fokker 50I show a similar trend as for the Saab 340T. The change in pitching moment due to propeller thrust is slightly under predicted, especially at higher flap deflections, but still follows the trend reasonably well. The fact that the error increases for higher flap deflections indicates that the flap lift prediction by AVL is not entirely correct. Which is an expected result as AVL only predicts a plain flap system, rather than more advanced flap systems typically implemented.

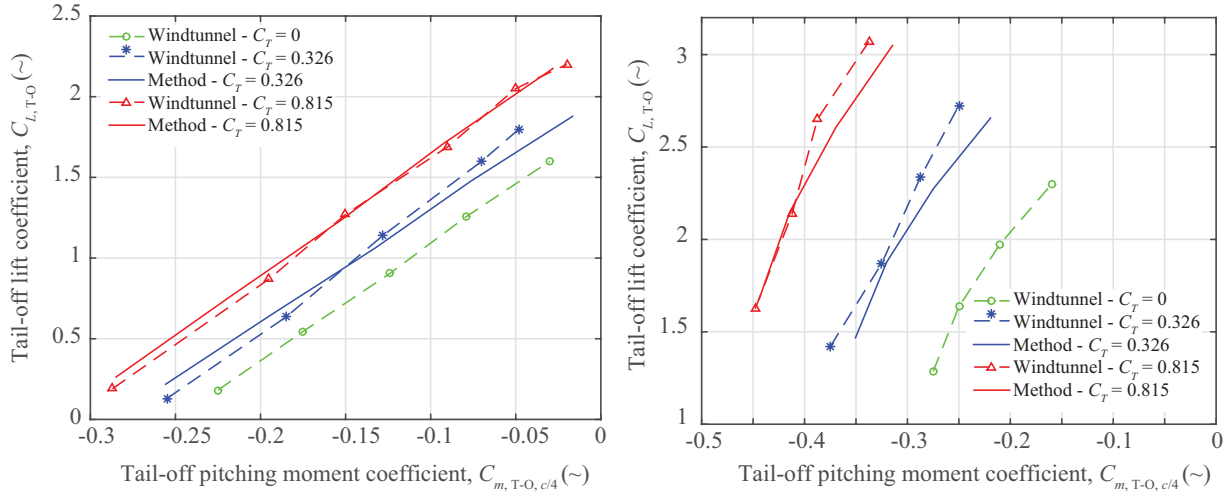


(a) Flaps 16.5 degrees

(b) Flaps 40 degrees

**Figure 11. Tail-off pitching moment curves - Fokker 50I**

## IV. Interpretation of Results

In this section, the results of the previous section are further interpreted and discussed to come to a better understanding of the capabilities of the method and the impact of the propeller slipstream on the lift and pitching moment of the aircraft.

### A. Tail-Off lift coefficient

The graphs in Figures 8 and 9 show the total effect of rotating propellers on the tail-off lift coefficient. A breakdown of the tail-off lift coefficient in its individual components is given in Table 2 for the Saab 340T at $\delta_f = 20°$ and $C_T = 0.6$. This breakdown lists the four variables calculated as described in Section A for four different angles of attack as well as the power-off and total power-on lift coefficient.

**Table 2. Calculated tail-off lift coefficients for the Saab 340T with flaps deflected 20 degrees and thrust coefficient of 0.6**

| angle-of-attack, $\alpha$ (deg) | -4 | 0 | 4 | 8 |
|---|---|---|---|---|
| Power-off lift, $C_{L_{\text{P-O}}}$ (~) | 0.574 | 0.971 | 1.344 | 1.690 |
| Wing lift minus slipstream, $C_{L_{\text{W-S}}}$ (~) | 0.558 | 0.945 | 1.308 | 1.645 |
| Lift due to slipstream, $C_{L_{\text{S}}}$ (~) | 0.306 | 0.381 | 0.458 | 0.528 |
| Propeller Normal Force, $C_{L_{\text{P}}}$ (~) | 0.004 | 0.017 | 0.030 | 0.043 |
| Vertical thrust component, $C_{L_{\text{T}}}$ (~) | -0.045 | 0 | 0.045 | 0.090 |
| Total Power-on lift, $C_L$ (~) | 0.824 | 1.344 | 1.839 | 2.305 |

It can be seen that the total lift coefficient is increased by an average of 38% with respect to the power-off condition. This could also be seen from Figure 8(b) and clearly confirms the importance of determining the propeller slipstream effect whilst designing a propeller aircraft. One important result from Table 2 is the fact that the majority (a minimum of 78% at an 8 degrees angle-of-attack) of the lift increase due to propeller thrust is caused by the increased flow velocity over the slipstream section of the wing ($C_{L_S}$). In fact, at -4 degrees angle-of-attack, the lift-due-to-slipstream is responsible for 116% of the increase in lift. This shows that the one-engine-inoperative case in take-off condition can have drastic effect on the lateral lift balance causing the aircraft to roll. Furthermore, it can be observed that the increase in lift is proportional to the propeller thrust coefficient. This means that the propeller slipstream effect will be strongest during take-off, where the thrust is maximum due to the low aircraft velocity.

## B. Tail-Off Pitching Moment Coefficient

The graphs in Figures 10 and 11 show the pitching moment on the $x$-axis as well as the lift coefficient on the $y$-axis. It can be observed that the tail-off pitching moment becomes more negative (nose down) due to rotating propellers according to the calculations and wind tunnel measurements. The pitching moment becomes more nose down because the increase in lift over the slipstream section is applied aft of the moment reference center. Interestingly, the effect of propeller thrust reduces for higher angles of attack. At higher angles of attack, the positive pitching moment caused by the propeller normal force and the upwash caused by the fuselage and nacelles reduce the nose down pitching moment effect.

Furthermore, the effect explained above becomes stronger for higher thrust coefficients as expected, but also for higher flap deflections. The flap deflection has an influence due to the fact that deflected flaps cause the increase in lift over the slipstream section of the wing to become larger and that the point of application of the lift force vector on the wing moves further aft.

## C. Tail-On Pitching Moment Coefficient

The horizontal tail pitching moment contribution ($C_{m_\mathrm{h}}$) versus angle-of-attack curves are calculated. The horizontal tail pitching moment is dependent on the downwash and average dynamic pressure at the tail. These variables are themselves dependent on the vertical distance between the horizontal tail and the slipstream center line. As the Fokker 50I and Saab 340T differ in tail height, a significant difference is expected in tail pitching moment. Figure 12 shows the effect of the propeller slipstream on the horizontal tail pitching moment for three different flap deflections of the Saab 340T. These graphs show that the difference between the power-on and power-off pitching moment contributions increases for higher flap deflections.

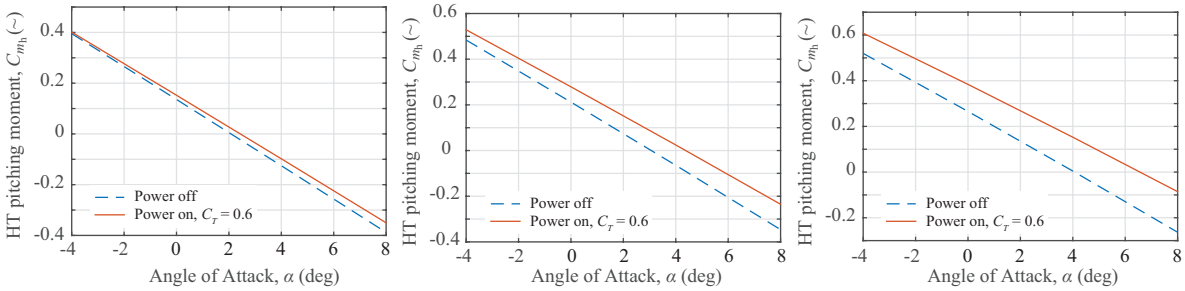


(a) Flaps retracted (b) Flaps 20 degrees (c) Flaps 40 degrees

**Figure 12. Horizontal tail pitching moment - Saab 340T**

The Fokker 50I has a low horizontal tail configuration. This low tail configuration leads to additional effects acting on the tail pitching moment as can be seen in Figure 13. Similar to the Saab 340, these figures show the effect of propeller thrust on the tail pitching moment for three different flap deflections. Although the power-off curves show a similar negative linear trend as before, the power-on curves are drastically different. This difference occurs because of the nonlinear dynamic pressure and downwash inflow effects. Furthermore, this difference also depends on the flap deflection.

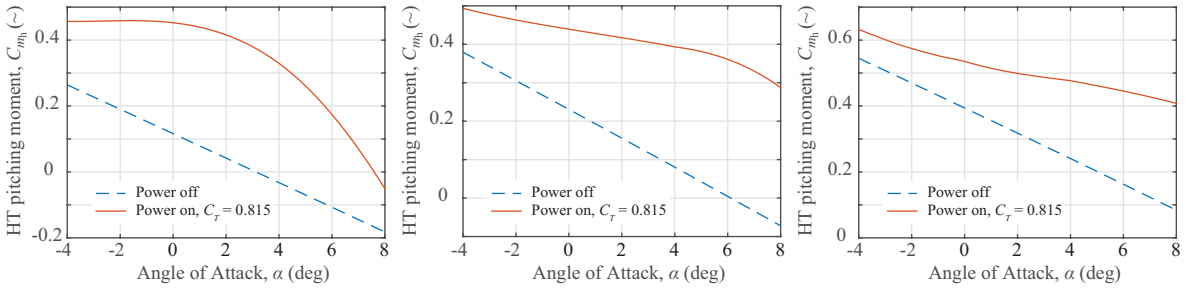


(a) Flaps retracted (b) Flaps 16.5 degrees (c) Flaps 40 degrees

**Figure 13. Horizontal tail pitching moment - Fokker 50I**

Using Equation 25 for the Saab 340T, results in a negative linear curve for the power-off and power-on conditions. As the distance between the tail and the slipstream center line in the power-on condition is greater than the contracted propeller slipstream diameter, no nonlinear inflow effects on the downwash or dynamic pressure increases occur. Therefore, the variation in downwash is only dependent on the lift coefficient, which varies linearly with respect to the angle-of-attack as shown in the graphs of Figure 8. Furthermore, the lift coefficient increases for increasing propeller thrust, resulting in a higher downwash angle. Because of this, the tail experiences a lower effective angle-of-attack ($\alpha_R - \varepsilon + i_h$). The lower effective angle-of-attack reduces the effectiveness of the tail due to a reduction in stabilizing negative (nose-down) pitching moment at higher angles of attack.

The Fokker 50I results are more complicated. Whilst the power-off results are similar to the Saab 340, the power-on results vary non-linearly with the angle-of-attack due to the inflow effect and dynamic pressure increase. The inflow effect occurs in the mixing region on the boundary of the contracted slipstream tube. As the angle-of-attack in the graphs of Figure 13 increases, the vertical distance between the tail and slipstream center line ($h$) changes. Therefore, the average downwash due to inflow increases, resulting in a less effective horizontal tail. More specifically, the maximum average downwash due to inflow occurs at different angles of attack for the three respective flap deflections. This is because the vertical distance ($h$) is dependent on the flap trailing edge position. For angles of attack beyond the angle-of-attack for maximum average downwash, the downwash gradient ($\mathrm{d}\varepsilon/\mathrm{d}\alpha$) decreases. This translates to an increase in tail effectiveness.

The average dynamic pressure ratio ($q_\mathrm{h}/q$), is also a function of $h$ and the ratio between the slipstream diameter and the tail span. An increase in dynamic pressure at the tail increases the lift over the tail. It follows naturally that an increase in dynamic pressure thus increases the effectiveness of the horizontal tail. This can be seen through a steeper tail pitching moment curve. For the three flap deflections shown in Figure 13, the maximum dynamic pressure ratio occurs for the case with the flaps retracted. With flaps retracted, the slipstream center line is not deflected by the flaps, and the vertical distance $h$ is lowest.

In terms of effectiveness, the tail is most effective with the flaps retracted beyond an angle-of-attack of 2 degrees. This is a result a high dynamic pressure ratio in combination with a low downwash gradient at the horizontal tail. For increased flap deflections the tail becomes progressively less effective due to the reduced dynamic pressure and increased downwash gradient. The difference in the horizontal tail pitching moment contribution with flap deflection, tail position, and thrust coefficient demonstrates the importance of properly capturing the propeller slipstream effect during the conceptual design of the horizontal tailplane.

## V. Conclusions

A semi-analytical method to predict the effect of the propeller slipstream on lift and pitching moment has been investigated. This method was tested against wind tunnel data of a T-tailed Saab 340 and a Fokker 50. It was shown that the effect of the propeller slipstream on the tail-off lift coefficient was well captured for both aircraft at various flap settings and thrust coefficients. Although less validation data was available for the tail-on case, the tail-off and tail-on predictions of the pitching moment coefficient were shown to be acceptable for the use during the conceptual design phase. Interpretation of the results showed that the propeller slipstream effect increases the lift coefficient up to 38%. Furthermore, the slipstream effect creates an additional nose-down pitching moment of the aircraft-less-tail. Furthermore, it was shown that the vertical position of the horizontal tail is affected by the slipstream due to the effect of downwash from the wing and increased dynamic pressure in the slipstream. Positioning the horizontal tail close to the center line of the slipstream causes large nonlinearities in the pitching moment contribution of the horizontal tail plane with angle-of-attack. This demonstrates that modeling the propeller slipstream effects is important for sizing of the horizontal tail plane in the conceptual design stage. Although further validation is still necessary, the method presented in this paper has been shown to be adequate for this task.

## Acknowledgements

The authors wish to acknowledge the large contribution of professor emeritus ir. Ed Obert, who has developed the presented methodology and has provided the authors with wind tunnel data to compare to. Furthermore, the authors wish to acknowledge the help of ir. Nando van Arnhem for providing critical feedback on the method and its implementation.

# References


[1]Phillips, W., *Mechanics of Flight*, Wiley, 2004, ISBN:9780471334583.

[2]Veldhuis, L., *Propeller wing aerodynamic interference*, TU Delft, Delft University of Technology, 2005, ISBN:9090195378.

[3]Theodorsen, T., "The theory of propellers - Part III, The slipstream contraction with numerical values for two-blade and four blade propellers," *NACA Report*, Vol. 777, 1944.

[4]Obert, E., "The Effect of Propeller Slipstream on the Static Longitudinal Stability and Control of Multi-Engined Aircraft," *Proceedings of the International Council of the Aeronautical Sciences' 19th Congress*, Anaheim, CA, September 1994, p. 7.3.4.

[5]De Young, J., "Propeller at high incidence," *Journal of Aircraft*, Vol. 2, No. 3, 1965, pp. 241–250, ISSN:0021-8669.

[6]Anon., *In-plane forces and moments on installed inclined propellers at low forward speeds*, IHS, 2006, ESDU data sheet 89047.

[7]Anon., *Introduction to installation effects on thrust and drag for propeller-driven aircraft*, IHS, 1986, ESDU data sheet 85015.

[8]Stepniewski, W., "Exprience tire des essais en vol d'un appareil VTOL a aile basculante." *Technique et Science Aeronautiques*, Vol. No. 1, 1960.

[9]Roskam, J. and Lan, C., *Airplane Aerodynamics and Performance*, Design, Analysis and Research Corporation, 1997, ISBN = 9781884885440.

[10]Campbell, J. and McKinney, M., "NACA Report 1098 - Summary of Methods for Calculating Dynamic Lateral Stability and Response and for Estimating Lateral Stability Derivatives," Report, National Advisory Committee for Aeronautics, 1952.

[11]Drela, M. and Youngren, H., "Athena Vortex Lattice," 2010.

[12]Obert, E., "The Effect of Propeller Slipstream on the Longitudinal Characteristics of a Model of the Saab 2000." unpublished appendix to Delft Aerospace Report LR-761.

[13]Obert, E., "The Effect of Propeller Slipstream on the Longitudinal Characteristics of a Model of the Saab 340 with a T-tail," unpublished appendix to Delft Aerospace Report LR-761.

[14]Jansen, Q. and Vos, R., "Assessing the Effect of Decreased Longitudinal Stability on Aircraft Size and Performance," *54th AIAA Aerospace Sciences Meeting*, San Diego, CA, 4-8 January 2015, pp. 1–16.